

Supporting information

Nickel phosphide decorated with trace amount of platinum as an efficient electrocatalyst for the alkaline hydrogen evolution reaction

Jiawei Xia,^{a,b} Kapil Dhaka,^c Michael Volokh,^b Guiming Peng,^b Zhen Wu,^a Yongsheng Fu,^a Maytal Caspary Toroker,^{*c} Xin Wang^{*a} and Menny Shalom^{*b}

^aKey Laboratory of Soft Chemistry and Functional Materials, Nanjing University of Science and Technology, Ministry of Education, Nanjing 210094, China.

^bDepartment of Chemistry and Ilse Katz Institute for Nanoscale Science and Technology, Ben-Gurion University of the Negev, Beer-Sheva 8410501, Israel.

^cDepartment of Materials Science and Engineering, Technion-Israel Institute of Technology, Haifa 3200003, Israel.

*Corresponding Author

Email: maytalc@technion.ac.il; wangx@njust.edu.cn; mennysh@bgu.ac.il

Table S1. Selected summary of HER performances of heteroatom doped Ni-P electrocatalysts.

Entry	Catalyst	Electrolyte	Current density (mA cm ⁻²)	Overpotential (mV)	Tafel slope (mV dec ⁻¹)	Metal doping (wt%)	Reference
1	Ni-P-Pt _{0.5} /Ni foam	1 M KOH	10	34	31	0.28	This work
2	Ni-P-Pt _{0.5} /Ni foam	1 M KOH	50	55	31	0.28	This work
3	Ni-P-Pt _{0.5} /Ni foam	0.5 M H ₂ SO ₄	10	48	36	0.28	This work
4	(Ni _{0.33} Fe _{0.67}) ₂ P	1 M KOH	50	214	–	~24	[1]
5	Ni-Fe-P nanocubes	1 M KOH	10	182	92	~25	[2]
6	FeNi _x /nickel foam	1 M KOH	100	161	80	–	[3]
7	P-NiFe@ nickel foam	1 M KOH	10	75	67	–	[4]
8	Co-Ni-P/Ti foil	1 M KOH	10	103	67	~40	[5]
9	CoP ₃ /Ni ₂ P	0.5 M H ₂ SO ₄	10	115	49	~26	[6]
10	NiCoP/carbon cloth	1 M KOH	10	62	68.2	–	[7]
11	Mn-Ni ₂ P nanosheets/ carbon cloth	0.5 M H ₂ SO ₄	10	97	45	–	[8]
12	Mn-Ni ₂ P/nickel foam	1 M KOH	10	103	135	–	[9]
13	Mo-Ni ₂ P/nickel foam	1 M KOH	10	78	109	~25	[10]
14	MoP/Ni ₂ P/nickel foam	1 M KOH	10	75	100.2	–	[11]
15	NiMoO-SP/Ti foil	1 M KOH	10	157	77	–	[12]

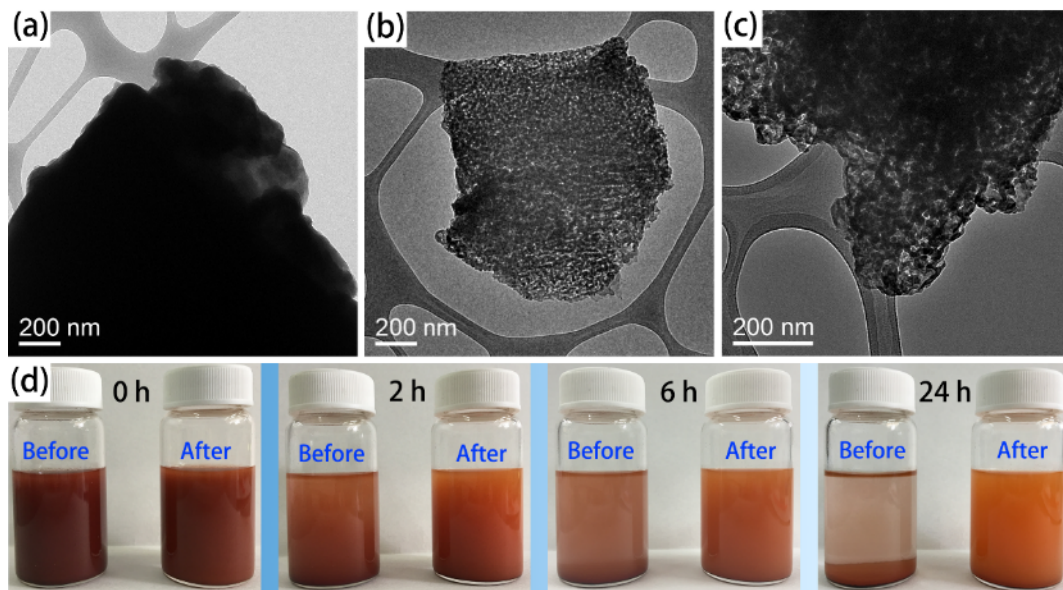


Fig. S1. (a) TEM image of red phosphorus, as received from manufacturer; (b–c) TEM images of pretreated red phosphorus at different magnifications; (d) Comparison of the dispersion of red phosphorus in 2-propanol before and after pretreatment.

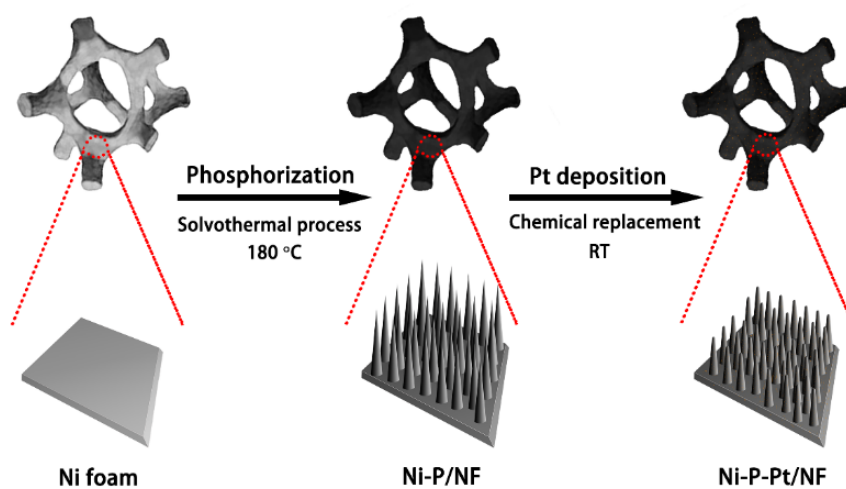


Fig. S2. Synthetic procedure of Ni-P-Pt/NF electrocatalysts.

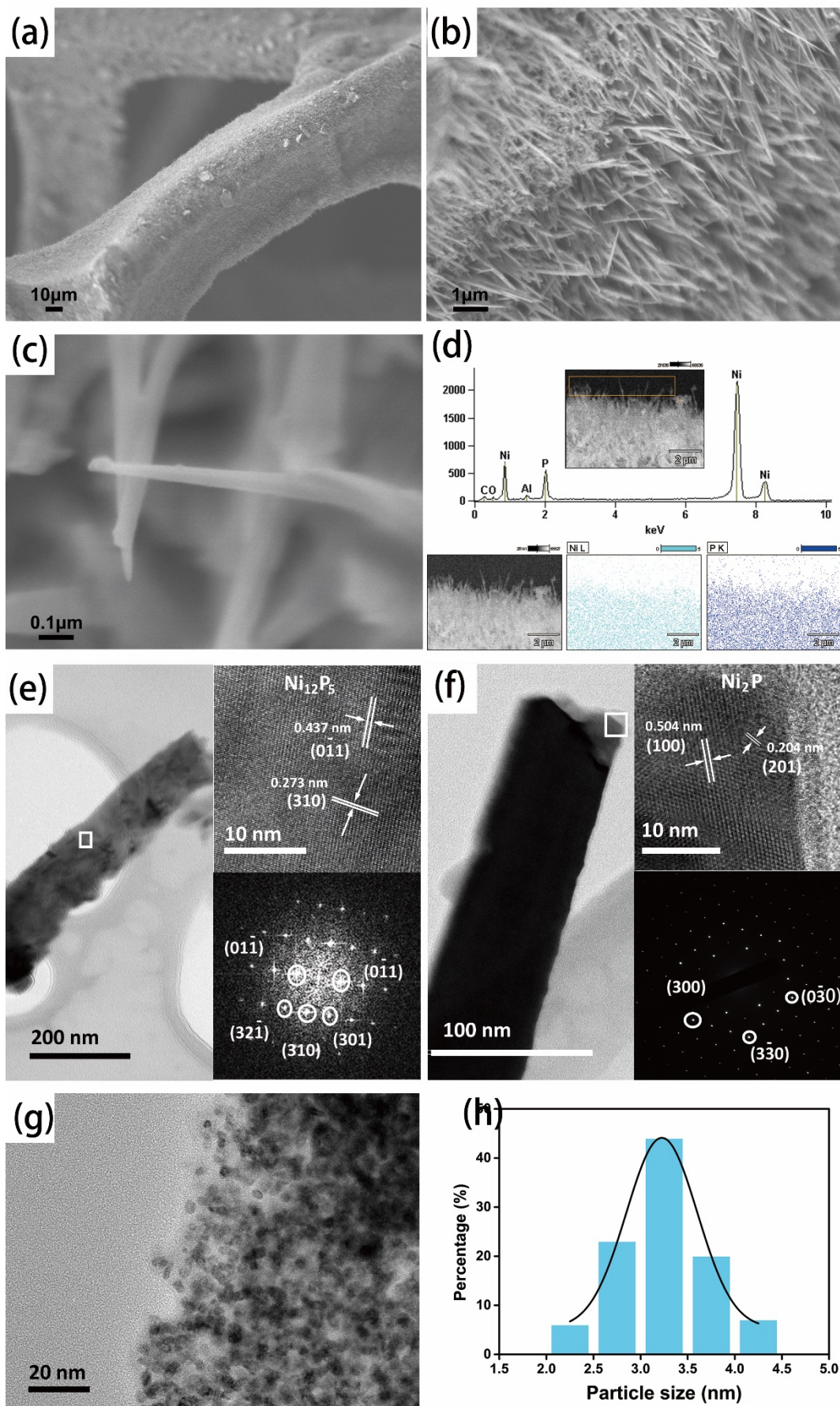


Fig. S3. (a–c) SEM images of Ni-P/NF catalyst prepared in ETA at different magnifications; (d) EDX spectrum and EDX elemental mapping images of Ni-P/NF catalyst prepared in ETA; (e) TEM and HRTEM images of Ni-P/NF at the middle of the sample, and an FFT analysis (from [-133] zone axis) obtained from HRTEM image (sample was prepared in ETA); (f) TEM, HRTEM and related SAED (from [001] zone axis) images of Ni-P/NF at the edge of the sample (sample was prepared in ETA); (g) TEM image of Ni-P-Pt_{0.5}/NF; (h) Pt size distribution of Ni-P-Pt_{0.5}/NF.

We note that due to thickness limitation we conducted selected-area electron diffraction (SAED) only at the edge of the sample. The interplanar spaces of 0.437 and 0.273 nm in Fig. S3e correspond to the (0-11) and (310) lattice planes of Ni₁₂P₅. The interplanar spaces of 0.504 and 0.204 nm in Fig. S3f correspond to the (100) and (201) lattice planes of Ni₂P.

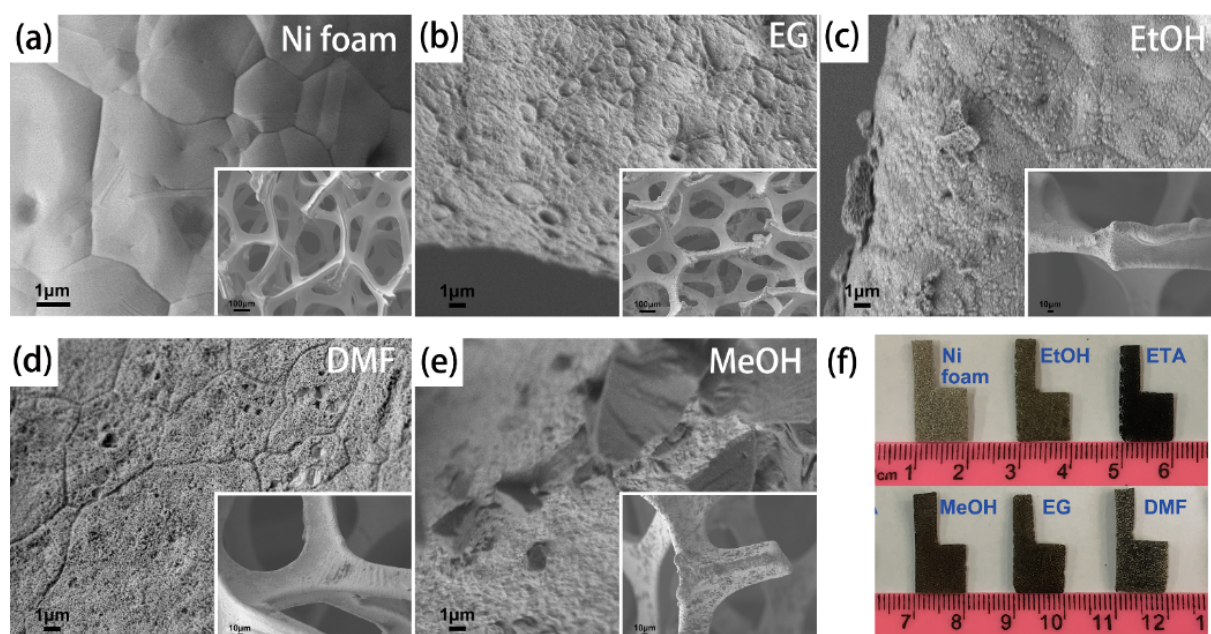


Fig. S4. (a–e) SEM images of Ni foam and Ni-P/NF catalysts prepared in EG, EtOH, DMF, and MeOH, respectively; (f) Digital images of the Ni foam and Ni-P/NF catalysts prepared in different solvents.

Among the reaction media investigated, Ni-P with a needle-like structure can only be formed in ethanolamine (ETA); they are expected to have a larger surface area and better catalytic activity than that of other structures (Fig. S2a–c). As for the other reaction media that were tested, namely ethylene glycol (EG), ethanol (EtOH), *N,N*-dimethylformamide (DMF), and methanol (MeOH), the smooth NF surface becomes rough, irregularly covered with Ni-P after phosphorization (Fig. S4).

Table S2. Pt content of Pt/NF and Ni-P-Pt/NF catalysts measured by ICP-AES.

Catalyst	Pt content (wt%)	Catalyst	Pt content (wt%)
Pt _{0.1} /NF	0.0063	Ni-P-Pt _{0.1} /NF	0.097
Pt _{0.2} /NF	0.0077	Ni-P-Pt _{0.2} /NF	0.14
Pt _{0.5} /NF	0.011	Ni-P-Pt _{0.5} /NF	0.28
Pt _{1.0} /NF	0.019	Ni-P-Pt _{1.0} /NF	0.48

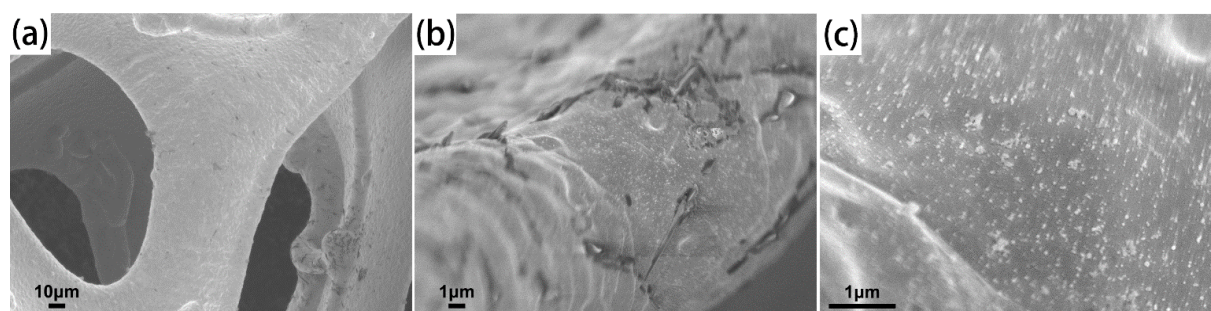


Fig. S5. SEM images of Pt_{0.5}/NF catalyst at different magnifications.

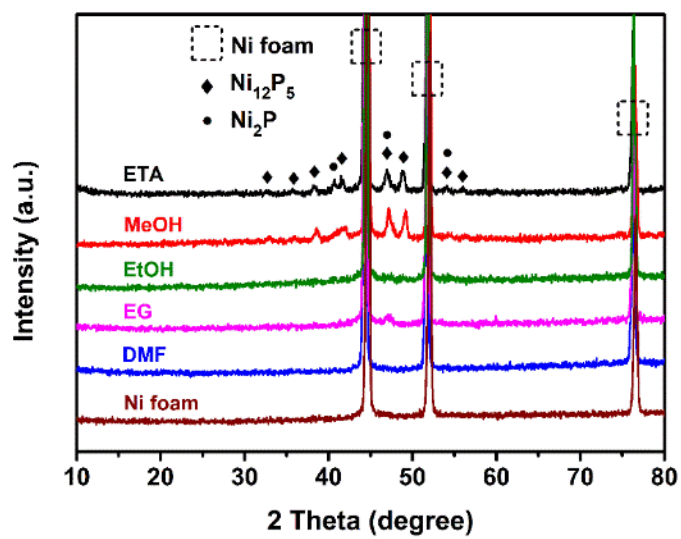


Fig. S6. XRD patterns of Ni-P/NF catalysts prepared in different solvents.

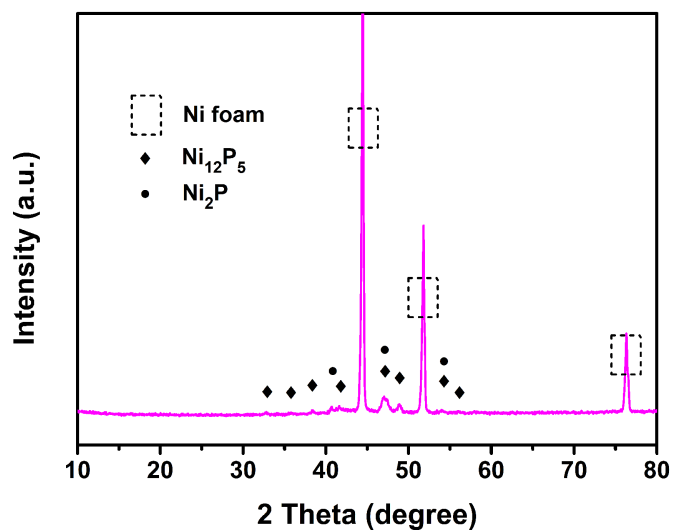


Fig. S7. XRD pattern of Ni-P/NF catalyst prepared in ETA for 20 h.

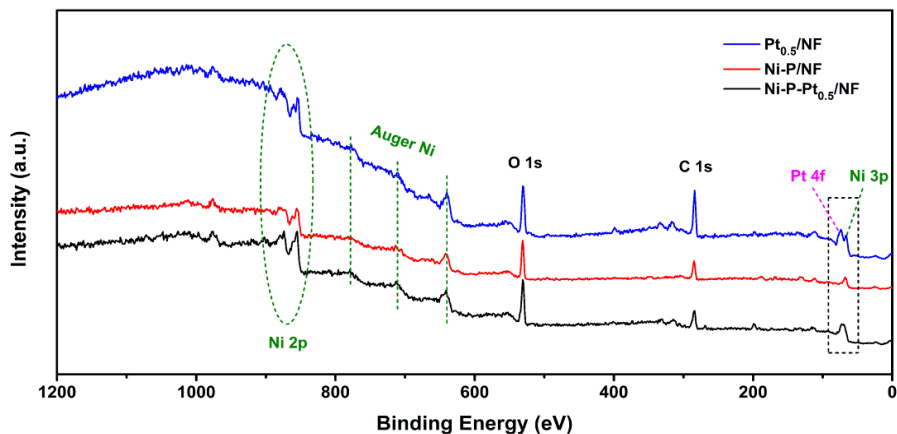


Fig. S8. Global XPS spectra of Pt_{0.5}/NF, Ni-P/NF and Ni-P-Pt_{0.5}/NF catalysts. The C 1s peaks are from the conductive carbon adhesive.

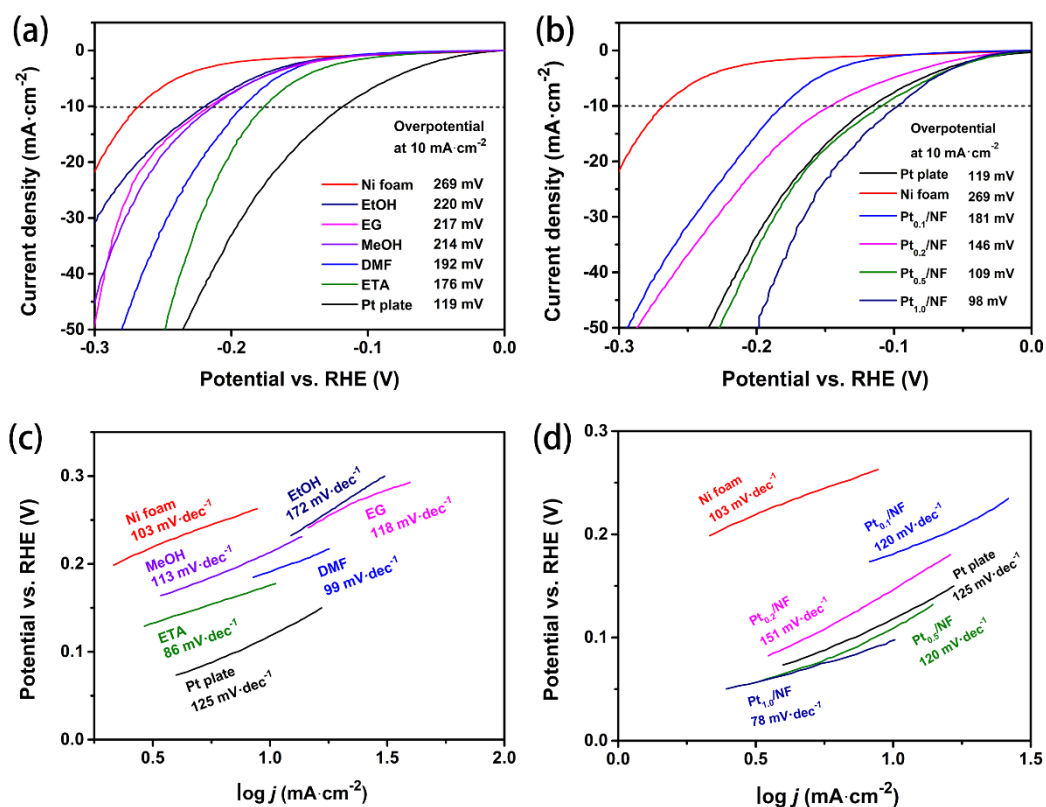


Fig. S9. (a–b) Linear sweep voltammetry (LSV) curves of Ni-P/NF and Pt/NF catalysts for HER in 1 M KOH aqueous solution (*iR* corrected); (c–d) Corresponding Tafel plots catalyzed by Ni-P/NF and Pt/NF in a 1 M KOH aqueous solution.

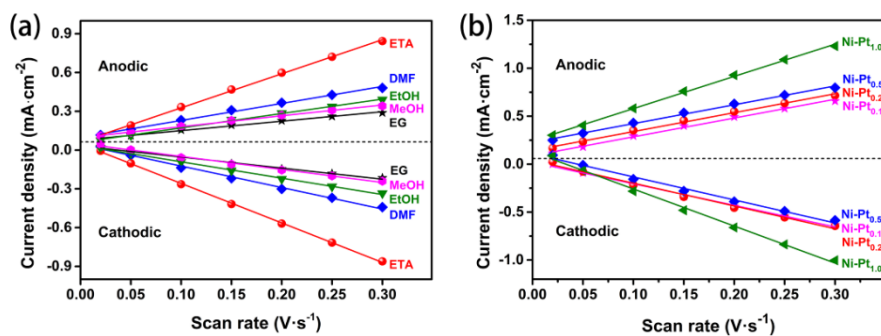


Fig. S10. Plots of cathodic and anodic current density of (a) Ni-P/NF and (b) Pt/NF changing with potential scan rates at 0 V vs. Ag/AgCl.

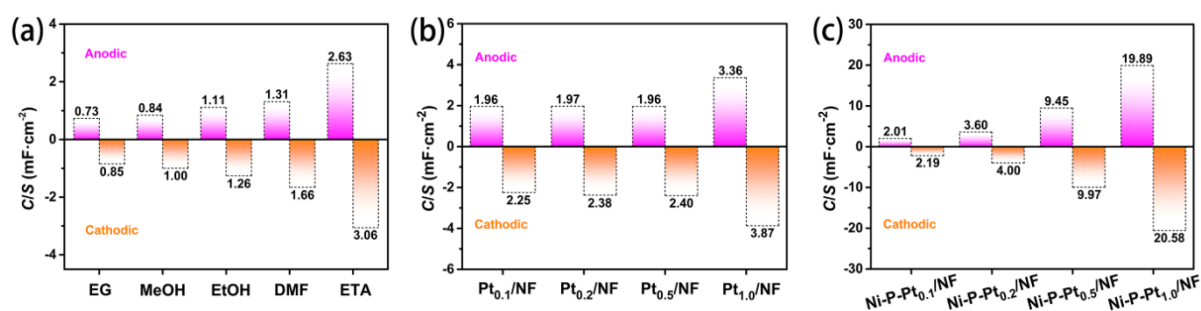


Fig. S11. Double-layer capacitance values of (a) Ni-P/NF catalysts made in different solvents; (b) Pt/NF and (c) Ni-Pt/NF catalysts.

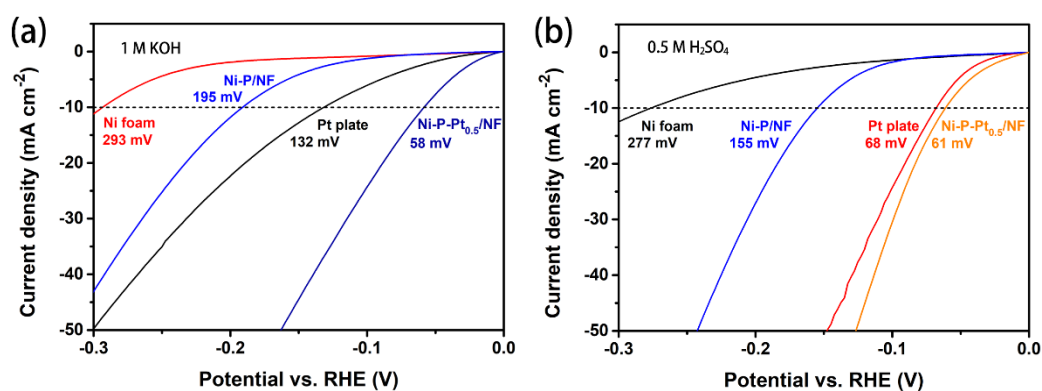


Fig. S12. Linear sweep voltammetry (LSV) curves of Ni foam, Pt plate, Ni-P/NF and Ni-P-Pt_{0.5}/NF catalysts for HER in (a) 1 M KOH and (b) 0.5 M H₂SO₄ aqueous solutions (before *iR* correction), respectively.

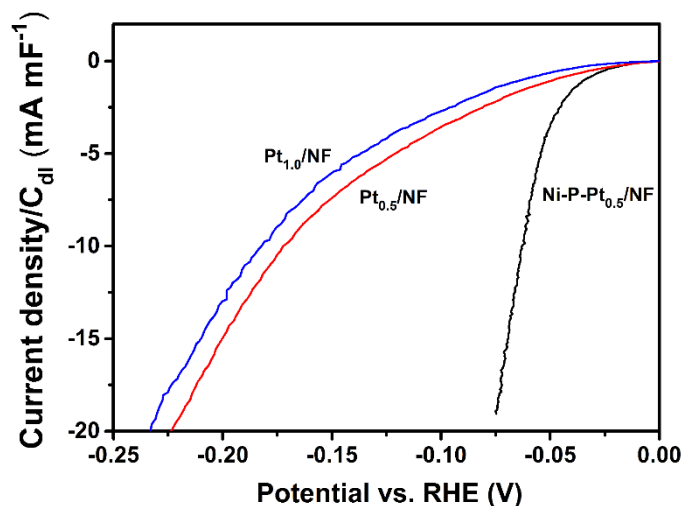


Fig. S13. LSV polarization curves of Pt_{1.0}/NF, Pt_{0.5}/NF, and Ni-P-Pt_{0.5}/NF catalysts referring to each electrochemical active surface area.

Table S3. Selected summary of HER performances of noble metal-based catalysts in 1 M KOH aqueous solution.

Entry	Catalyst	Current density (mA cm ⁻²)	Overpotential (mV)	Tafel slope (mV dec ⁻¹)	Reference
1	Ni-P-Pt _{0.5} /Ni foam	10	34	31	This work
2	Ni-P-Pt _{0.5} /Ni foam	50	55	31	This work
3	Ni foam/Pt-C	10	50	37.8	[13]
4	Pt nanowires/single layer Ni(OH) ₂	2.48	70	—	[14]
5	Pt/C (20%)	10	47	46	[10]
6	Pt/C (20%)	50	75	46	[10]
7	Pt ₃ Ni ₃ nanowire	10	50	—	[15]
8	RuP ₂ @NPC	10	52	69	[16]
9	RuO ₂ /Co ₃ O ₄	10	89	91	[17]

Table S4. Price calculation of Ni-P-Pt_{0.5}/NF, Pt plate and commercial Pt/C catalysts.

Entry	Catalyst	Price1 (USD cm ⁻²)	Price 2 (USD g ⁻¹)
1	Ni-P-Pt _{0.5} /NF	0.003350	0.09040
2	Pt plate (1 cm × 1 cm × 0.01 cm)	5.867	27.35
3	Commercial Pt/C (20 wt% of Pt)	0.003870 ^a	5.471 ^a

a) Basic information:

Price: Ni: 6.380 USD lb⁻¹ = 0.01407 USD g⁻¹

Pt: 850.8 USD oz⁻¹ = 27.35 USD g⁻¹

Prices retrieved from “<http://www.infomine.com/investment/metal-prices/>”, date: 17/07/2018.

For the price calculation of commercial Pt/C, we consider that 5 mg mL⁻¹ dispersion of Pt/C is prepared first, and then 10 μL is taken out and dropped onto the glassy carbon electrode (diameter of 3 mm). Here we only calculate the price of Pt without carbon.

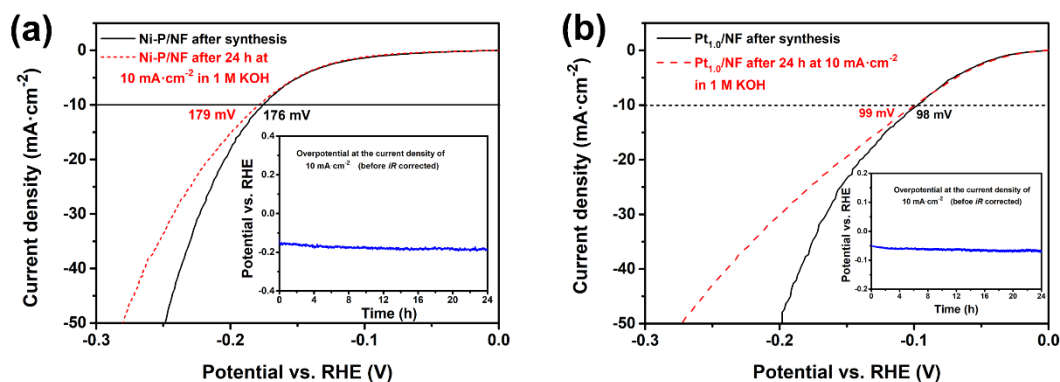


Fig. S14. LSV curves of (a) Ni-P/NF and (b) Pt_{1.0}/NF for HER before and after a 24-h durability test in 1 M KOH aqueous solution (*iR* corrected), the insets show the corresponding potential changing with time at a current density of 10 mA cm⁻². All the durability tests were conducted with graphitic rod as the counter electrode.

Here, in order to eliminate the influence of dissolved Pt coming from the Pt plate, a graphite rod was employed as the counter electrode during the whole durability measurement. Meanwhile, stirring at 200 rpm was used to remove the bubbles on the surface of catalysts.

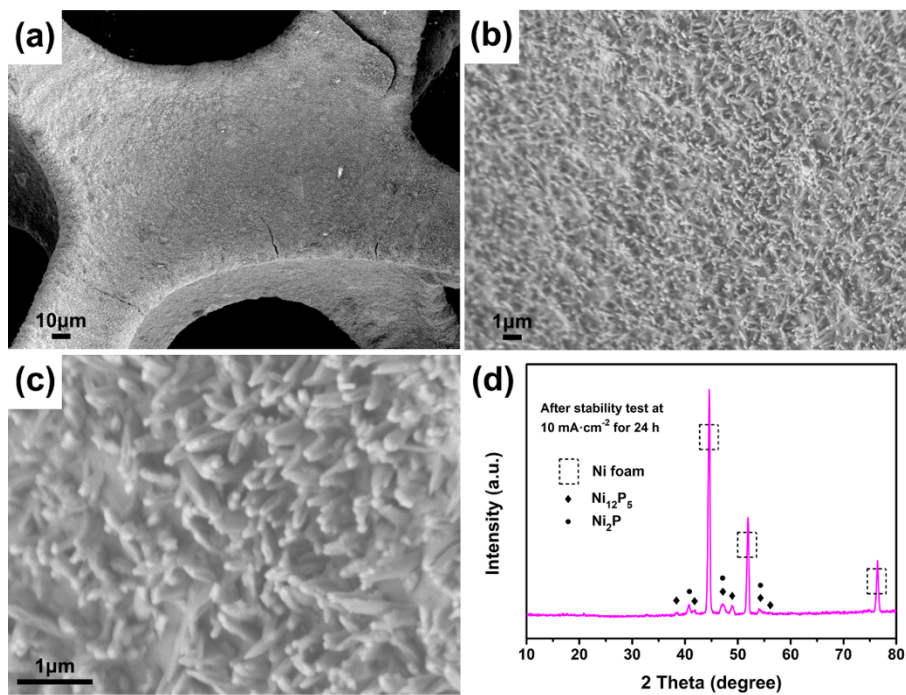


Fig. S15. (a–c) SEM images of Ni-P-Pt_{0.5}/NF catalyst at different magnifications after HER durability test. (d) XRD pattern of Ni-P-Pt_{0.5}/NF after HER durability measurement.

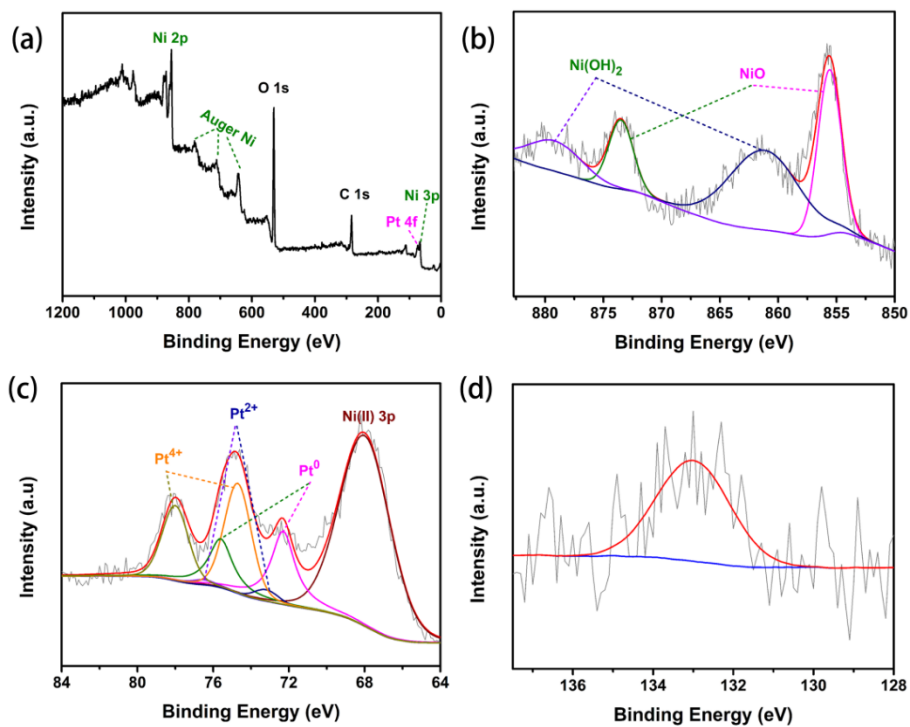


Fig. S16. (a) Global XPS spectrum, (b) Ni, (c) Pt, and (d) P high-resolution XPS spectra of Ni-P-Pt_{0.5}/NF catalyst after durability measurement.

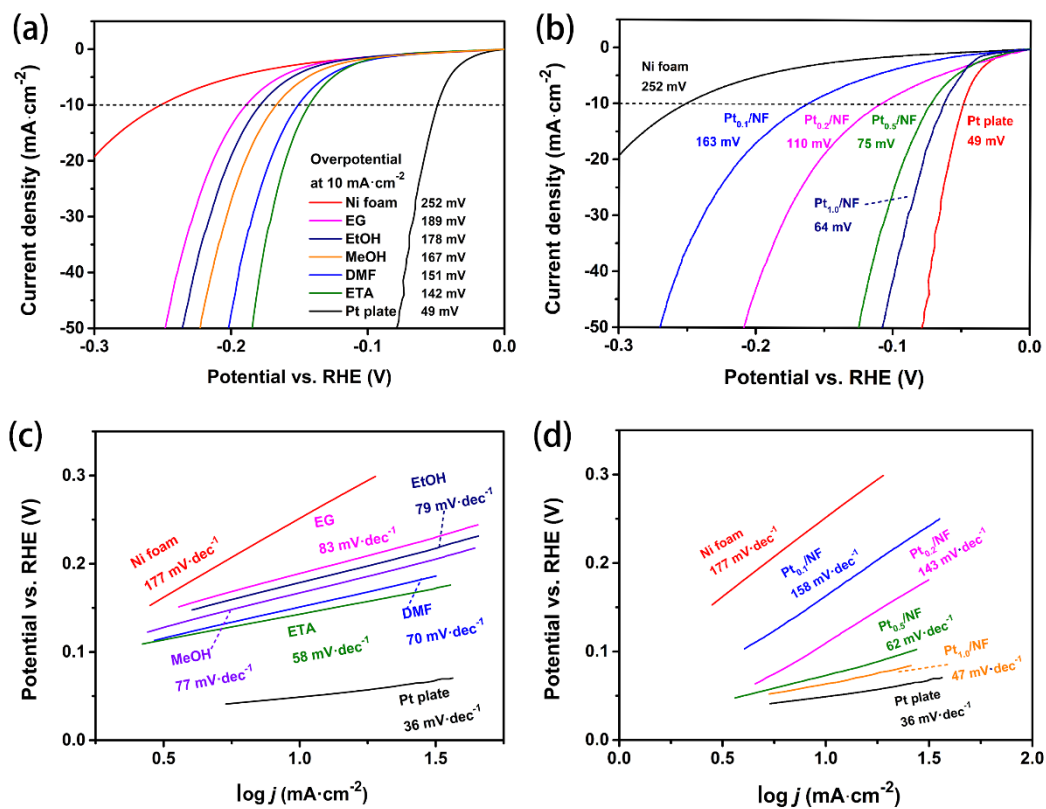


Fig. S17. (a–b) LSV curves of Ni-P/NF and Pt/NF catalysts for HER in 0.5 M H₂SO₄ aqueous solution (*iR* corrected); (c–d) Corresponding Tafel plots catalyzed by Ni-P/NF and Pt/NF in 0.5 M H₂SO₄ aqueous solution.

DFT computational details:

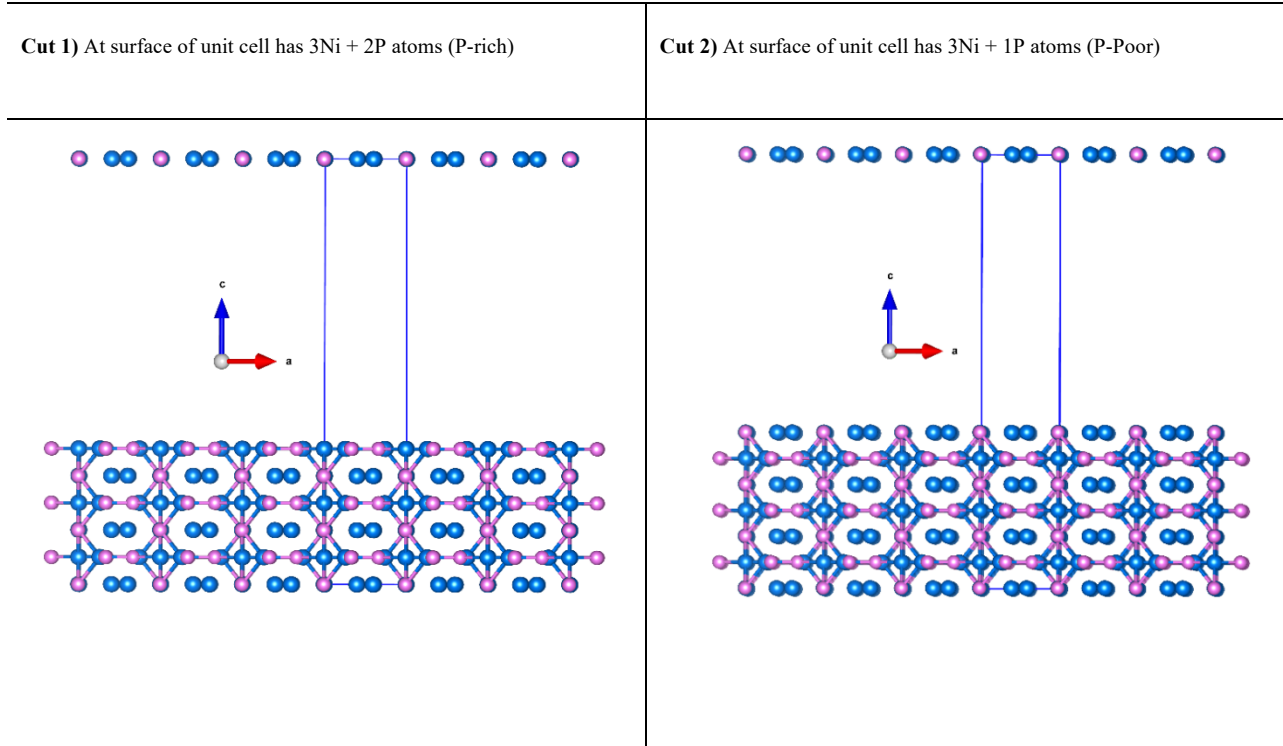
Spin-polarized DFT (Density Functional Theory) calculations were performed with the Vienna Ab Initio Simulation Package (VASP).^{18,19} We use the Perdew-Burke-Ernzerhof (PBE)²⁰ of the general gradient approximation (GGA) exchange-correlation (XC) functional in all computational calculations. This functional describes well to all the chosen transition metal complexes.²¹⁻²⁴ Projected augmented wave (PAW) potentials^{25,26} represented all frozen core electrons and nuclei for each atom. The KS equations were solved with a plane-wave basis set to self-consistency under three-dimensional periodic boundary conditions. Symmetry operations were imposed for a better description of the interface geometry. We used a k-mesh of $4 \times 4 \times 1$ gamma point and an energy cutoff of 600 eV for the plane-wave basis set. These k-grid's and energy cutoffs were converged to a total energy within 1 meV atom⁻¹. For all the calculations, we relaxed the cells using a convergence criterion of 10^{-6} eV for electronic iterations and 0.03 eV Å⁻¹ for ionic iterations. Geometrical relaxations took place with a conjugate gradient algorithm. All slabs were separated from their periodic image by a minimum of 14 Å vacuum layers which is converged the total energy up to 0.1 meV atom⁻¹.

DFT calculation results:

Nickel phosphide (Ni₂P), which adopts a hexagonal Fe₂P structure, is a well-known catalyst for HER reactions. For DFT calculation, initially we examined the structure of bulk Ni₂P. The following is DFT/PBE-optimized bulk lattice constants a , b , and c of Ni₂P. N_a is the number of atoms in the bulk unit cell.

	Space group	a [Å]	b [Å]	c [Å]	N_a
Ni ₂ P	P 1 (Triclinic)	5.88	5.88	3.37	9

For Ni₂P (001), initially, there are two kinds of cuts possible as follows:



To obtain the most favorable hydrogen coverage of the surfaces under the steady-state conditions of the HER we analyzed the change of the Gibbs free surface energy upon hydrogen adsorption:

$$\Delta\gamma = \frac{1}{A_{nm}} [E_{\text{slab}}^{m \times n}(N_{\text{H}}) - E_{\text{slab}}^{m \times n}(0) - N_{\text{H}}\mu_{\text{H}}]$$

where, N_{H} is the number of absorbed hydrogen atoms and μ_{H} is the concentration-dependent chemical potential, A is the area of $n \times m$ surface of the unit cell, n and m is defining the size of the surface unit cell. We use the total energy of the H₂ gas phase molecule E_{H_2} as zero point of energy by introducing $\mu_{\text{H}} = \Delta\mu_{\text{H}} + \frac{1}{2}E_{\text{H}_2}$. Here, the upper limit is set for hydrogen chemical potential to $\Delta\mu = 0$.

Differential hydrogen adsorption energies are defined by

$$E_{\text{ad}}^{\text{diff}} = E_{\text{slab}}^{m \times n}(N_{\text{H}}) - E_{\text{slab}}^{m \times n}(N_{\text{H}} - 1) - \frac{1}{2}E_{\text{H}_2}$$

They are converted to hydrogen adsorption free energies via

$$\Delta G_{\text{H}} = E_{\text{ad}}^{\text{diff}} + \Delta E_{\text{ZPE}} - TS = E_{\text{ad}}^{\text{diff}} + 0.24 \text{ eV}$$

Since the differential hydrogen adsorption energies ΔE_H is the function of differential adsorption free energies ΔG_H as $\Delta G_H = \Delta E_H + 0.24$ eV, where +0.24 eV is the entropy and zero-point energy contributions which is constant for hydrogen molecules.

Cut 1:

P-rich: Ni₂P (001) Surface:

Hydrogen coverages are given in monolayers (ML), with one ML corresponding to one H per surface Ni atom. Since both P-rich and P-poor surfaces have three surface Ni atoms, we have gradually covered with H atoms to find the reaction rate at each adsorption.

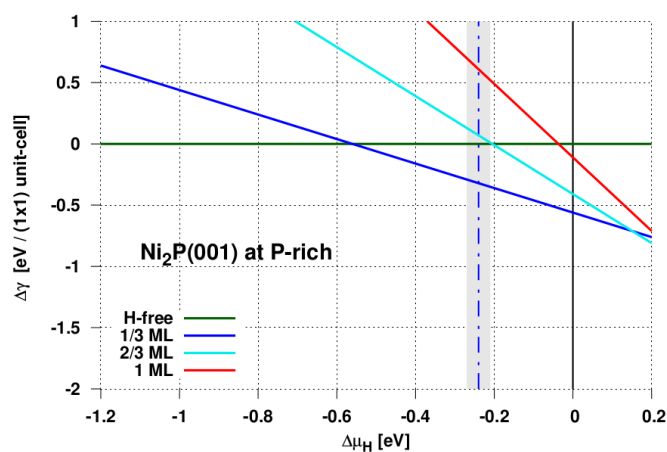


Fig. S18. Surface phase diagram of hydrogen adsorbed at P-rich: Ni₂P (001). The hydrogen chemical potential under HER conditions (at -0.24 eV hydrogen chemical potential) is indicated by a vertical dashed blue line.

P-rich: Ni₂P (001)-1Pt Surface:

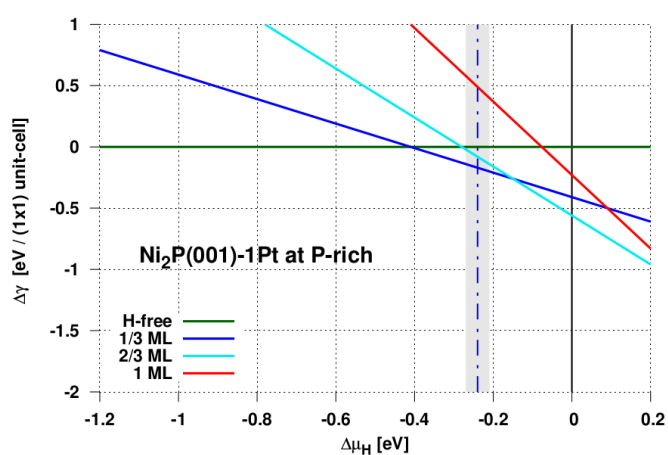


Fig. S19. Surface phase diagram of hydrogen adsorbed at P-rich: Ni₂P (001)-1Pt (one surface Ni atom is replaced by one Pt atom). The hydrogen chemical potential under HER conditions (at -0.24 eV) is indicated by a vertical dashed blue line.

P-rich: Ni₂P (001)-2Pt Surface:

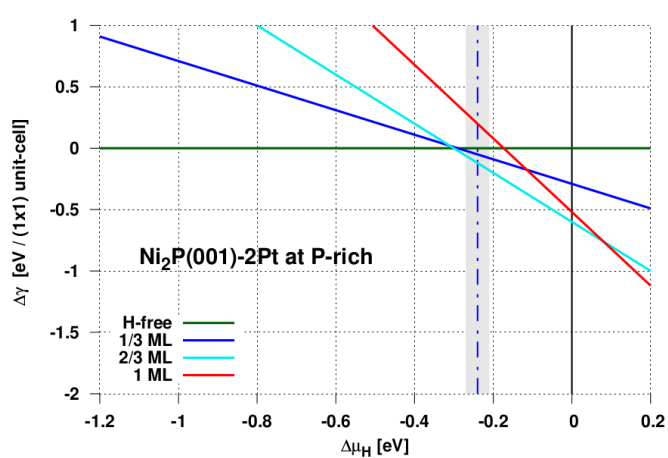


Fig. S20. Surface phase diagram of hydrogen adsorbed at P-rich: Ni₂P (001)-2Pt (2 surface Ni atoms are replaced by 2 Pt atoms). The hydrogen chemical potential under HER conditions (at -0.24 eV) is indicated by a vertical dashed blue line.

P-rich: Ni₂P (001)-3Pt Surface:

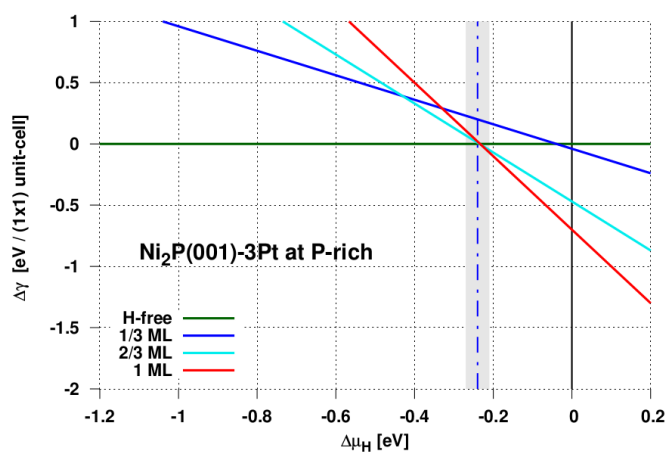


Fig. S21. Surface phase diagram of hydrogen adsorbed at P-rich: Ni₂P (001)-3Pt (3 surface Ni atoms are replaced by 3 Pt atoms). The hydrogen chemical potential under HER conditions (at -0.24 eV) is indicated by a vertical dashed blue line.

Cut 2:

P-poor: Ni₂P (001) Surface:

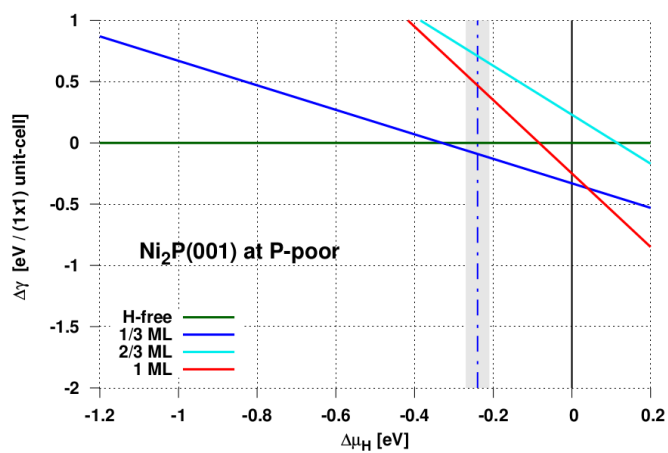


Fig. S22. Surface phase diagram of hydrogen adsorbed at P-poor: Ni₂P (001). The hydrogen chemical potential under HER conditions (at -0.24 eV) is indicated by a vertical dashed blue line.

P-poor: Ni₂P (001)-1Pt Surface:

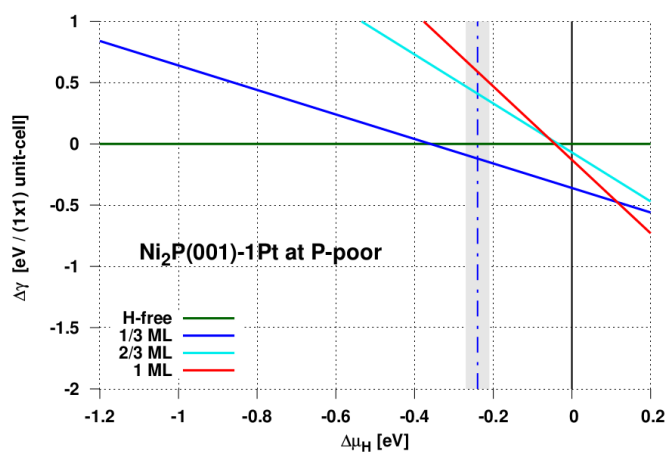


Fig. S23. Surface phase diagram of hydrogen adsorbed at P-poor: Ni₂P (001)-1Pt (one surface Ni atom is replaced by one Pt atom). The hydrogen chemical potential under HER conditions (at -0.24 eV) is indicated by a vertical dashed blue line.

P-poor: Ni₂P (001)-2Pt Surface:

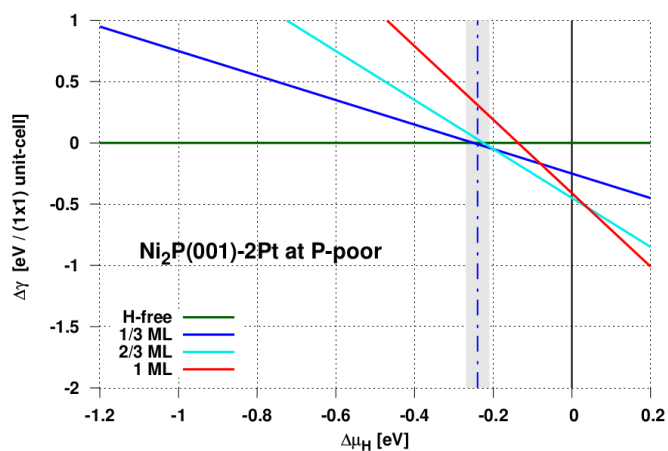


Fig. S24. Surface phase diagram of hydrogen adsorbed at P-poor: Ni₂P (001)-2Pt (2 surface Ni atoms are replaced by 2 Pt atoms). The hydrogen chemical potential under HER conditions (at -0.24 eV) is indicated by a vertical dashed blue line.

P-poor: Ni₂P (001)-3Pt Surface:

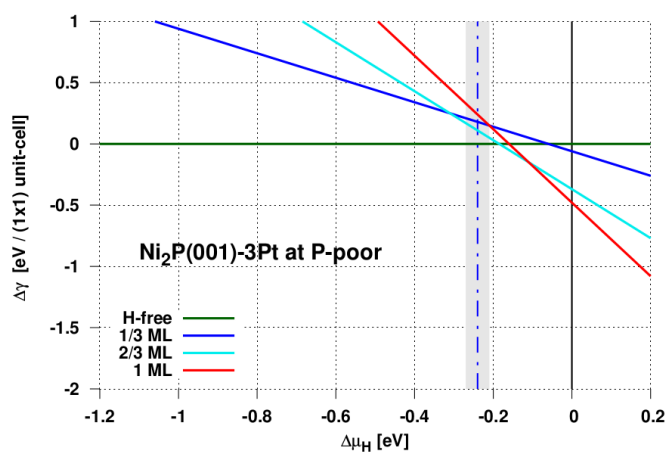


Fig. S25. Surface phase diagram of hydrogen adsorbed at P-poor: Ni₂P (001)-3Pt (3 surface Ni atom are replaced by 3 Pt atoms). The hydrogen chemical potential under HER conditions (at -0.24 eV) is indicated by a vertical dashed blue line.

Table S5. Differential hydrogen adsorption energy and hydrogen adsorption free energy ΔG_H for the thermodynamically most favorable surface structure under HER conditions as derived from the phase diagram in Fig. S18–S25.

Figure	Initial Coverage [ML]	Final Coverage [ML]	E_{ad}^{diff} [eV]	ΔG_H [eV]
S18	1/3	2/3	0.15	0.39
S18	2/3	1	0.30	0.54
S19	1/3	2/3	-0.15	0.09
S19	2/3	1	0.33	0.57
S20	1/3	2/3	-0.31	-0.07
S20	2/3	1	0.08	0.32
S21	1/3	2/3	-0.44	-0.20
S21	2/3	1	-0.23	0.01
S22	1/3	2/3	0.56	0.80
S22	2/3	1	-0.47	-0.23
S23	1/3	2/3	0.29	0.53
S23	2/3	1	-0.06	0.18
S24	1/3	2/3	-0.20	0.04
S24	2/3	1	0.04	0.28
S25	1/3	2/3	-0.31	-0.07
S25	2/3	1	-0.11	0.13
DFT results from Ref [27,28]		Pt (111)		0.11

To find the improvement in HER activity by adding Pt atoms, we examined the reaction rate which is calculated by the following expression:

$$r = k_0 \frac{\exp\left(\frac{\Delta G_H}{kT}\right)}{1 + \exp\left(\frac{\Delta G_H}{kT}\right)}$$

Using this expression, we have calculated current densities with the function of free energies of the considered surface structures in the HER volcano in Fig. 5 in the main paper.

Bader charge analysis:

To understand the charge distribution and charge transfer as observed from the experiments, we calculated the Bader charge of Ni₂P (001) surfaces with and without Pt atoms using DFT. All the distributed charge results are summarized in Tables S6–S7 below.

Table S6 and S7 suggest that charge is transferred from P to Pt atoms. Also, from the zero magnetization on Pt, we can determine the oxidation state of Pt should be +2.

Table S6. Bader charges on surface atoms for P-rich Ni₂P (001) surface. Since there are 3Ni and 2P atoms on the P-rich surface, Pt atoms replace surface Ni atoms one by one.

	Ni ₂ P (001)	Ni ₂ P (001)-1Pt	Ni ₂ P (001)-2Pt	Ni ₂ P (001)-3Pt
Ni(1)	0.10	—	—	—
Ni(2)	0.10	0.09	—	—
Ni(3)	0.10	0.09	0.06	—
P(1)	-0.22	-0.04	0.19	0.39
P(2)	-0.22	-0.04	0.19	0.39
Pt(1)	—	-0.46	-0.44	-0.40
Pt(2)	—	—	-0.43	-0.45
Pt(3)	—	—	—	-0.41

Table S7. Bader charges on surface atoms for P-poor Ni₂P (001) surface. Since there are 3Ni and 1P (plus 1P atom is adopted from inner layer) atoms on the P-poor surface, Pt atoms replace surface Ni atoms one by one.

	Ni ₂ P (001)	Ni ₂ P (001)-1Pt	Ni ₂ P (001)-2Pt	Ni ₂ P (001)-3Pt
Ni(1)	0.19	—	—	—
Ni(2)	0.19	0.21	—	—
Ni(3)	0.19	0.21	0.22	—
P(1)	-0.36	-0.18	0.04	0.29
P(2)-adopted from inner layer	-0.36	-0.26	-0.16	-0.08
Pt(1)	—	-0.32	-0.29	-0.27
Pt(2)	—	—	-0.29	-0.27
Pt(3)	—	—	—	-0.27

Supporting Information References:

- [1] Y. Li, H. Zhang, M. Jiang, Q. Zhang, P. He and X. Sun, *Adv. Funct. Mater.*, 2017, **27**, 1702513.
- [2] C. Xuan, J. Wang, W. Xia, Z. Peng, Z. Wu, W. Lei, K. Xia, H L. Xin and D. Wang, *ACS Appl. Mater. Interfaces*, 2017, **9**, 26134–26142.
- [3] C. Xiao, B. Zhang and D. Li, *Electrochim. Acta*, 2017, **242**, 260–267.
- [4] F. S. Zhang, J. W. Wang, J. Luo, R. R. Liu, Z. M. Zhang, C. T. He and T. B. Lu, *Chem. Sci.*, 2018, **9**, 1375–1384.
- [5] Y. Pei, Y. Yang, F. Zhang, P. Dong, R. Baines, Y. Ge, H. Chu, P. M. Ajayan, J. Shen and M. Ye, *ACS Appl. Mater. Interfaces*, 2017, **9**, 31887–31896.
- [6] K. Wang, X. She, S. Chen, H. Liu, D. Li, Y. Wang, H. Zhang, D. Yang and X. J. Yao, *Mater. Chem. A*, 2018, **6**, 5560–5565.
- [7] C. Du, L. Yang, F. Yang, G. Cheng and W. Luo, *ACS Catal.*, 2017, **7**, 4131–4137.
- [8] X. Wang, H. Zhou, D. Zhang, M. Pi, J. Feng and S. Chen, *J. Power Sources*, 2018, **387**, 1–8.
- [9] Y. Zhang, Y. Liu, M. Ma, X. Ren, Z. Liu, G. Du, A. M. Asiri and X. Sun, *Chem. Commun.*, 2017, **53**, 11048–11051.
- [10] Y. Sun, L. Hang, Q. Shen, T. Zhang, H. Li, X. Zhang, X. Lyu and Y. Li, *Nanoscale*, 2017, **9**, 16674–16679.
- [11] C. Du, M. Shang, J. Mao and W. Song, *J. Mater. Chem. A*, 2017, **5**, 15940–15949.
- [12] Y. Wang, T. Williams, T. Gengenbach, B. Kong, D. Zhao, H. Wang and C. Selomulya, *Nanoscale*, 2017, **9**, 17349–17356.
- [13] G. F. Chen, T. Y. Ma, Z. Q. Liu, N. Li, Y. Z. Su, K. Davey and S. Z. Qiao, *Adv. Funct. Mater.*, 2016, **26**, 3314–3323.

- [14] H. Yin, S. Zhao, K. Zhao, A. Muqsit, H. Tang, L. Chang, H. Zhao, Y. Gao and Z. Tang, *Nat. Commun.*, 2015, **6**, 6430.
- [15] P. Wang, K. Jiang, G. Wang, J. Yao and X. Huang, *Angew. Chem. Int. Ed.*, 2016, **55**, 12859–12863.
- [16] Z. Pu, I.S. Amiinu, Z. Kou, W. Li and S. Mu, *Angew. Chem. Int. Ed.*, 2017, **129**, 11717–11722.
- [17] H. Liu, G. Xia, R. Zhang, P. Jiang, J. Chen and Q. Chen, *RSC Adv.*, 2017, **7**, 3686–3694.
- [18] G. Kresse and J. Hafner, *Phys. Rev. B*, 1993, **48**, 13115.
- [19] G. Kresse and J. Furthmüller, *Comput. Mater. Sci.*, 1996, **6**, 15–50.
- [20] J.P. Perdew, K. Burke and M. Ernzerhof, *Phys. Rev. Lett.*, 1996, **77**, 3865.
- [21] V. R. Stamenkovic, B. Fowler, B. S. Mun, G. Wang, P. N. Ross, C. A. Lucas and N. M. Marković, *Science*, 2007, **315**, 493–497.
- [22] F. Studt, F. Abild-Pedersen, T. Bligaard, R. Z. Sørensén, C. H. Christensen and J. K. Nørskov, *Science*, 2008, **320**, 1320–1322.
- [23] E. Nikolla, J. Schwank and S. Linic, *J. Catal.*, 2009, **263**, 220–227.
- [24] S. Sitthisa, W. An and D. E. Resasco, *J. Catal.*, 2011, **284**, 90–101.
- [25] G. Kresse and D. Joubert, *Phys. Rev. B*, 1999, **59**, 1758.
- [26] P. E. Blöchl, *Phys. Rev. B*, 1994, **50**, 17953.
- [27] J. K. Nørskov, T. Bligaard, A. Logadottir, J. R. Kitchin, J. G. Chen, S. Pandelov and U. Stimming, *J. Electrochem. Soc.*, 2005, **152**, J23–J26.
- [28] C. G. Morales-Guio, L. A. Stern and X. Hu, *Chem. Soc. Rev.*, 2014, **43**, 6555–6569.